Characterization and Application of Nanomaterials (2023) Volume 6 Issue 1
doi:10.24294/can.v6i1.2033

ORIGINAL RESEARCH ARTICLE

Decontamination of surface water from organic pollutants using graphene membranes

Stefano Bellucci

INFN-Laboratori Nazionali di Frascati, Via E. Fermi 54, Frascati 00044, Italy. E-mail: bellucci@lnf.infn.it

ABSTRACT

In this paper, we deal with one of the most urgent and relevant topics nowadays, i.e., water pollution. The problem is finding a valid candidate for the absorption and removal of different kinds of pollutants commonly found in water. There are already some indications about graphene oxide as a potential candidate. In the present work, we take a step forward to show how graphene nanoplatelets (rather than the oxide form of this material) are capable of decontaminating water. In this starting step, we use a specific substance as a model pollutant, i.e., acetonitrile, leaving for the future steps, to extend the analysis to additional types of pollutants. In addition to laboratory-produced graphene nanoplatelets, we already examined in the past; now we wish to consider also commercially available ones, so that the new results will not be bound to a laboratory (low technology readiness level) material, but will become interesting also from the industrial point of view, thanks to the scalability of the nanoplatelets production. For this aim, we compare the performance of two types of filters based on two classes of nanomaterials, i.e., those produced by microwave and ultrasound assisted exfoliation, already analyzed in our earlier works, with those commercially distributed by an Italian company, i.e., NANESA, http://www.nanesa.com/. The latter is an innovative SME involved in the production of graphene-based nanomaterials. We focus here in the graphene nanoplatelets, commercially available in industrial batches (GXNan grades). The present study leads to determine which filtering membrane, among the various types of commercial graphene considered, shows the greatest stability, and the lack of breakage of the membrane, concentrating on such accessory features, given that all types of graphene showed excellent adsorption properties.

Keywords: Water Decontamination; Graphene Nanoplatelets; Acetonitrile; Filtering Membranes

ARTICLE INFO

Received: 17 April 2023
Accepted: 8 June 2023
Available online: 19 June 2023

1. Introduction

One of the most important problems nowadays is the contamination of the environment and more specifically of surface and underground waters by toxic substances, e.g., heavy metals and organic pollutants. Shortage of supplies of potable water is occurring in many areas worldwide, owing to the steady increase of the population, yielding to the harsh exploitation of water resources by human activities, which introduce many contaminants, including organic dyes, heavy metal ions, salts of light metals. In order to contrast what has by now already turned into one of the most severe concerns in the world's community, it is necessary to carry out the decontamination of wastewater[1,2].

Graphene oxide (GO) is a valid candidate for the absorption and removal of pollutants in water. Recently, several articles have shown that synthetic GO has high adsorbing capacities towards dyes, antibiotics and heavy metals[3]. This is probably due to its large surface area and the presence of different functional groups containing oxygen on the surface, which make each atom of this element available to chelate the metal ion.

Further experiments were conducted with zinc ions, hypothesizing that the main force of absorption is ion exchange, while electrostatic interaction could also influence the process. In fact, the results show that the absorption depends strongly on the pH of the solution and slightly on the presence of foreign ions and the ionic strength of the solution. Also in this case, the thermodynamic parameters indicate a spontaneous and endothermic absorption[3].

Another form of graphene commonly used in literature is that of the graphene nanoplatelets (GNP), characterized by a number of sheets between 2 and 11, stacked on one another, which are often called double-, few-, or multi-layered graphene sheets. They are different both from the graphene, composed of a single layer of carbon, and from the graphite, which implies a structure of 8 or more sheets of graphene; they can therefore be considered an intermediate phase, with distinct properties that vary according to the number of layers, until the structure of the graphite is reached. GNPs are known as quasi-graphene, and precisely because their properties vary according to the number of sheets, it is good to specify the type of nanoplatelets with which one is working (i.e., to indicate the number of layers from which they are composed). Once the 8 layers have been overcome, the electronic properties of the structure change, being more similar to those of graphite, so in these cases the nanostructures are considered[4].

Such a low-cost type of graphene has already drawn great interest due to its potential use in large scale industrial production. It has also been used for water decontamination, using filters realized by a disk of pressed graphene nanoplatelets. In the study of Ferrigno *et al.*[5], the fabrication, modeling and experimental characterization of a monitorable and renewable pollution filter based on graphene nanoplatelets was considered. The main goal was to demonstrate a method to monitor the status of such a filter in real time during its operating phases: pollutant adsorption, saturation, and regeneration. The graphene nanoplatelets were obtained by exploiting the thermal expansion of commercial intercalated graphite. This exfoliation method, assisted by microwave irradiation, represents a low-cost and ecologically friendly method to obtain the needed nanomaterial. The filter was used here to adsorb acetonitrile, a water-soluble organic compound with a triple bond, widely adopted in industrial processes, as well as in some industrial solvents and paints.

The main results obtained in the study of Ferrigno *et al.*[5] were twofold. Firstly, the graphene filter was shown to be effective in adsorbing the selected pollutant, with the additional feature of being fully renewable: all the pollutant can be removed from the filter without the need of costly physical or chemical processes. Secondly, monitoring of the time-evolution of the electrical impedance allowed efficient detection of the different phases of the filter life cycle: clean, polluted, saturated and regenerated. Let us recall why the measurement of the membrane impedance parameter allows to understand the actual absorption (including possible evaporation) of the pollutant (e.g., acetonitrile). Indeed, the method proposed by Ferrigno *et al.*[5] when monitoring the electrical impedance filter in real time, during the filtering operation, relied upon the interpretation of the latter physical observable using an equivalent circuit model, thanks to the well-known high sensitivity of the graphene electrical properties to the presence of external elements adsorbed in its lattice. The variations of the filter's resistance thus provided the markers to the filter cycle: the peaks of such a variation indicated the start and the end of the adsorption, whereas the reduction of the standard deviation showed that the filter went back to be clean[5].

This article[6] proposed a similar approach, emphasizing the smart monitoring of the life cycle of the same kind of graphene nanoplatelets-based filters for water remediation in the presence of pollutants. The measurement technique was based on suitable figures of merit, analyzing the time variation of the electrical impedance frequency spectrum. The study of Miele *et al.*[6] considered, in addition to the acetonitrile, also the remediation of another toxic industrial pollutant, i.e., the 2,4-dichlorophenol.

It is well known that production of graphene nanoplatelets through liquid exfoliation, sonication and centrifugation of graphite in suitable solvents

is a practical approach to prepare graphene dispersions. In the study of Gomez *et al.*[7], a detailed experimental and theoretical investigation seeking to explain the liquid exfoliation of graphene in polar solvents at short sonication time was presented, demonstrating that the short-time exfoliation process can only be optimized by dispersing graphene in dimethylformamide (DMF) and that edge-type defects are most noticeable when graphene is exfoliated in ethanol. However, precisely the aim of our production with the assistance by microwave is the avoidance of such non-green chemical compounds.

The recent paper[8] studied the temperature dependence of the electrical resistivity of low-cost commercial graphene-based strips, made from a mixture of epoxy and commercial graphene nanoplatelets produced by NANESA[9]. The results suggest that such materials can be used as thermistors in sensing or heating applications. We considered the same commercial (NANESA) graphene nanoplatelets to prepare filters, by the procedure adopted by Ferrigno *et al.*[5] and Miele *et al.*[6], for the graphene nanoplatelets developed within the INFN Frascati Laboratories[10,11], where the anticorrosion properties of the INFN laboratory-grade nanoplatelets were explored, suitable for the adsorption of acetonitrile. The advantage of using commercially available nanomaterials is obvious, both for reducing the cost of the filters and the scaling-up of the process, to reach a higher level of technological maturity of the products for environmental remediation.

Clearly, the topic of water depollution from organic substances, we treat in this paper, has been the subject of extensive investigations over the years. A short list of the published works in this connection can be given as [12–24].

2. Materials and methods

The main activity concerned the creation of filters/membranes in graphene that have been used for the decontamination of surface waters polluted with agents of organic nature.

We considered essentially two types of filters to compare, consisting of:

- Graphene Nano-Platelets (GNP), developed within the INFN Frascati Laboratories[10];
- Graphene made available by NANESA (G2Nan, G3Nan, G4Nan and G7Nan)[9].

The standard procedure for filter creation follows the criteria described here.

An amount equal to 200 mg of GNPs/graphene Nanesa was prepared and dispersed in 400 mL of isopropyl alcohol inside a beaker (the choice of the solvent to be used fell on isopropyl alcohol, being the best from a cost/benefit point of view, in which GNPs are completely dispersed), as shown in **Figure 1**.

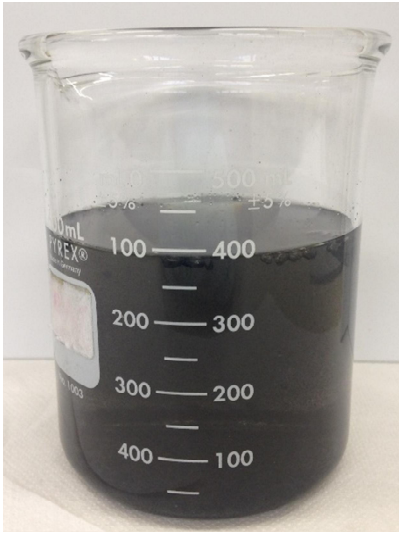

Figure 1. 200 mg graphene in 400 mL isopropyl alcohol.

The resulting solution was subjected to sonication through the use of the SONICS VibraCell ultrasonic tip. The ultrasonic tip was set in the following mode: a one-second pulse at 40% power alternating with a one-second rest for a total sonication time of 1 h; the choice of pulse mode and power are both optimal in order not to obtain excessive heating of the solution, also allows a good separation of the graphene planes (**Figure 2**).

Figure 2. Ultrasounds tip SONICS VibraCell.

Once sonication was finished, the solution was vacuum filtered using a PTFE (Polytetrafluoroethylene) filter with a porosity of 0.2 μm, which allows the passage of isopropyl alcohol molecules but not the dispersed nanoparticles, so that these can be deposited. Subsequently, the nanoparticle layer was collected and placed in an oven at 85 °C to allow complete evaporation of the isopropyl alcohol, whose evaporation temperature is 82.6 °C.

Finally, each GNP/grapheneNanesa membrane made by this procedure was pressed in an automated press with a force of 700 N.

Unfortunately, the properties belonging to the different types of commercial graphene do not allow us to use the same procedure previously used for Graphene Nano-Platelets (GNPs) of the INFN Frascati laboratories[10].

The changes made were as follows:

- **G2Nan:** As shown in **Figures 3** and **4**, the amount of graphene is sufficient to maintain the ratio 1:2 (200 mg graphene, 400 mL isopropyl alcohol). The negative note concerns the quality of the membrane, from the images is evident the presence of lumps and a non-homogeneous distribution of the material, which irreversibly damage the final product.

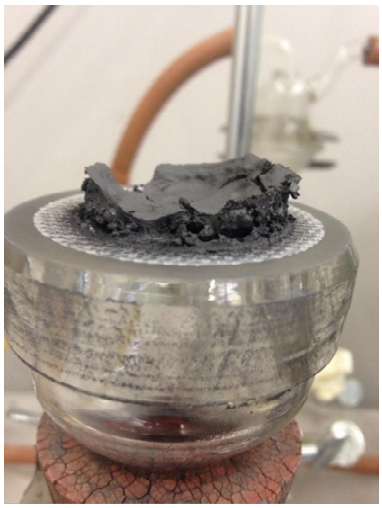

Figure 3. G2Nan Standard Procedure.

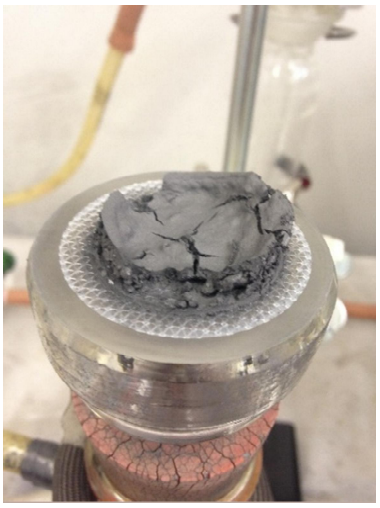

Figure 4. G2Nan Standard Procedure.

- To overcome these problems, we resorted to a prolonged sonication anticipated by the use of an additional instrument, the mechanical disperser IKA T10 basic ULTRA-TURRAX® (**Figures 5** and **6)**.

Figure 5. Mechanical disperser.

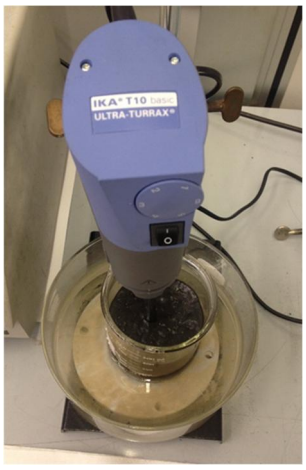

Figure 6. Mechanical disperser in action.

Standard procedure	G2Nan procedure
Ratio graphene/isopropyl alcohol **1:2**	Ratio graphene/isopropyl alcohol **1:2**
Mechanical dispersion **NO**	Mechanical dispersion **YES** (1 h, 10 min on/ 10 min off at power 3)
Sonication **1 h**	Sonication **2 h**

- **G3Nan:** As with G2Nan, the use of a mechanical disperser followed by a prolonged sonication phase is necessary (**Figure 7**). Moreover, a further problem results from the quantity of the product. In fact, 200 mg of graphene are not necessary to form a disc with adequate thickness (>0.5 mm). Therefore, it was decided to switch from a 1:2 ratio to a 1:1 one, thus inserting 400 mg of G3Nan inside 400 mL of isopropyl alcohol (**Figure 8**).

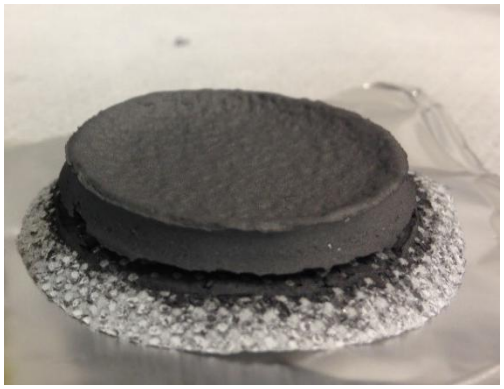

Figure 7. G3Nan 200 mg standard procedure.

Figure 8. G3Nan 400 mg standard procedure.

Standard procedure	G3Nan procedure
Ratio graphene/isopropyl alcohol **1:2**	Ratio graphene/isopropyl alcohol **1:1**
Mechanical dispersion **NO**	Mechanical dispersion **YES** (1 h, 10 min on/ 10 min off at power 3)
Sonication **1 h**	Sonication **2 h**

The reason for doubling the amount of G3Nan graphene compared to G2Nan could depend on the average particle lateral size (average particle lateral size), which for G2Nan is 30 µm while for G3Nan it is 15 µm.

- **G4Nan:** See the G3Nan procedure. In this case, we double the amount of graphene compared to G2Nan because of the bulk density, which for G2Nan is about 0.036 g/cm^3 (average between 0.020 and 0.042 g/cm^3), while for G4Nan is 0.07 g/cm^3. So, for the same weight, G2Nan will take up much more space than G4Nan. Differences between G4Nan discs at 200 mg and 400 mg are shown in **Figures 9** and **10**.

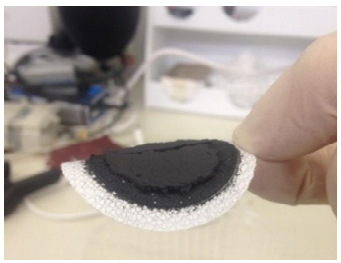

Figure 9. G4Nan 200 mg.

Figure 10. G4Nan 400 mg.

Standard procedure	G4Nan procedure
Ratio graphene/isopropyl alcohol **1:2**	Ratio graphene/isopropyl alcohol **1:1**
Mechanical dispersion **NO**	Mechanical dispersion **YES** (1 h, 10 min on/ 10 min off at power 3)
Sonication **1 h**	Sonication **2 h**

- **G7Nan:** With this last type of graphene, it was not possible to create discs/filters, because of the properties that characterize it. The apparent density (Bulk Density) is remarkable compared to the other products, equal to 0.2 g/cm^3, therefore a considerable weight was derived. In addition, the average lateral particle size (average particle lateral size) is extremely small (about 12 μm), giving G7Nan considerable fineness. Therefore, attempts to create a membrane using 200 mg, 400 mg, and 800 mg (thus with a 2:1 graphene/isopropyl alcohol ratio) of G7Nan were not sufficient (**Figures 11**, **12**, and **13**).

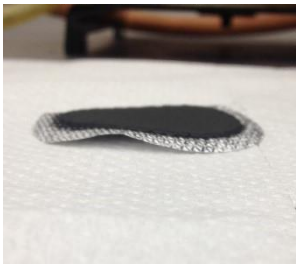

Figure 11. G7Nan 200 mg.

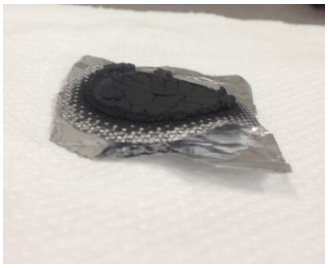

Figure 12. G7Nan 400 mg.

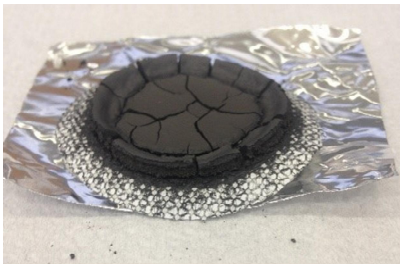

Figure 13. G7Nan 800 mg.

Once the filter formation procedure was completed, their ability to absorb acetonitrile (CH_3CN), the simplest organic nitrile, was evaluated. This was accomplished through the use of MFIA. The MFIA (from Zurich Instruments, Zurich, Switzerland) is a digital impedance analyzer and precision LCR meter that sets the new standard for impedance measurements in the frequency range of 1 MHz to 5 MHz. The MFIA features a basic accuracy of 0.05%, high measurement repeatability, and small temperature variation.

The MFIA meter was connected to the graphene membrane through metal rings used as "inductive plates" (**Figure 14**). The plates have an outer diameter of 4.5 cm, an inner diameter of 2.5 cm, and a thickness of 4 mm, perforated in the center to allow the insertion of a PPR (a type of plastic for plumbing uses) tube, into which acetonitrile is inserted during the experiment. The graphene membrane, being a conductor, is then inserted in contact with the two plates and the tube. By doing so, the set-up allows the measurement of the impedance parameter of the membrane, allowing in turn to understand the actual absorption (along with any evaporation) of the acetonitrile released during the experiment.

Figure 14. Inductive plates.

3. Results and discussion

Impedance measurements determined with the MFIA instrumentation involved the following steps:

- Once the membrane was inserted inside the inductive plates, the MFIA was operated, beginning to measure the impedance value for 30 min;

- After 30 min, 1 mL of acetonitrile was released inside the PPR tube leading directly to the membrane;
- Finally, the impedance was calculated for a minimum time of 2 h after release.

In **Table 1**, for each variety of commercial graphene, the thickness, the number of tests performed, and the weight change during the phases of the membrane use are specified.

Table 1. Thickness, number of tests performed, and weight change of the membrane

		G2Nan	**G3Nan**	**G4Nan**
Diameter		33.8 mm		
Thickness		0.8 mm	1.3 mm	0.7 mm
1st test	Initial weight	0.1948 g	0.3757 g	0.2318 g
	Final weight	0.1943 g	0.3757 g	0.2309 g
2nd test	Initial weight	0.1942 g	0.3757 g	0.2309 g
	Final weight	0.1942 g	0.3741 g	0.2270 g
3rd test	Initial weight	0.1942 g		0.2244 g
	Final weight	0.1941 g		0.2202 g

One can be puzzled about the reason why the thicknesses of the tested membranes differ significantly. This is due to the different characteristics (e.g., porosity) of the different types of graphene used, which yielded also in different values of the membrane mass, resulting from filtration. Nevertheless, there was no effect of the thickness on membrane fracture during testing. As one can see from the table:

- The diameter of the discs will always remain unchanged and equal to 33.8 mm, while the thickness will vary depending on the material (as has been seen before);
- As far as weight is concerned, a slight decrease is observed at each test performed, mainly caused by the fragile and extremely delicate nature of graphene, which involves minimal but inevitable losses every time the filter is handled to set-up. The decrease in weight is also an indication of total evaporation of the acetonitrile once the tests are completed;
- Finally, it must be taken into account that for the two filters G3Nan and G4Nan, the end of the second and third test (respectively) corresponds to the breakage of the filter itself, confirming once again the fragility of the product. With the exception of the membrane obtained using G2Nan, which is much more stable, a property that can be understood from the minimal weight variations with respect to the other two membranes.

The data released by MFIA measurements mainly provide the trend of the absolute value of the impedance

$$(Abs(Z) = |Z^I + jZ^{II}| = \sqrt{(Z^I)^2 + (Z^{II})^2}),$$

a function of frequency (with a range from 80 Hz to 1 MHz).

Three frequencies were taken as reference, in an attempt to cover the entire measured range. They are 50 kHz, 500 kHz and 1 MHz.

The graph in **Figure 15** shows the behavior of impedance as the frequency varies. The increase in frequency involves the formation, a few minutes after the release of acetonitrile, of a depression (probably due to the acceleration of the evaporation process due to higher frequencies). This trend was found for each type of graphene studied.

Figures 16–**21** show the behavior of Abs(Z) as time varies for the different tests performed, the frequencies taken into account will be 50 kHz and 1 MHz.

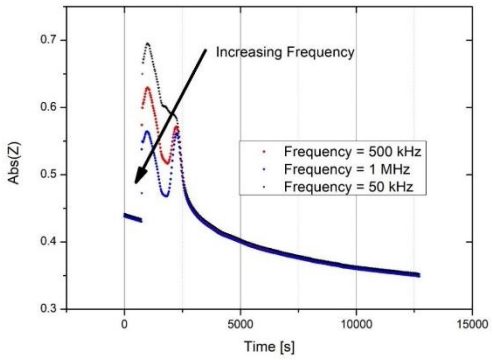

Figure 15. G4Nan, influence of frequency in the behavior of Abs(Z).

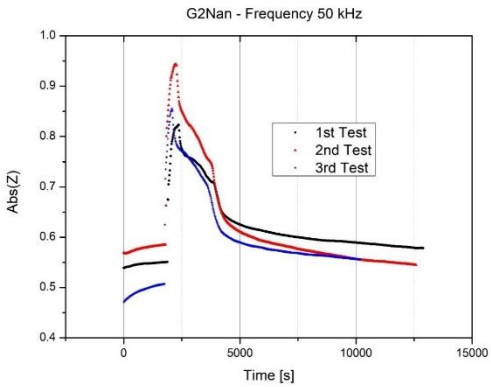

Figure 16. G2Nan, time dependence of Abs(Z) at 50 kHz.

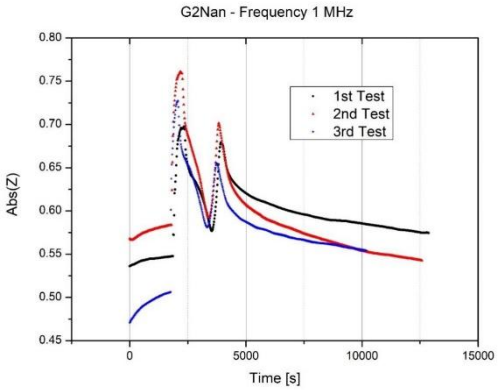

Figure 17. G2Nan, time dependence of Abs(Z) at 1 MHz.

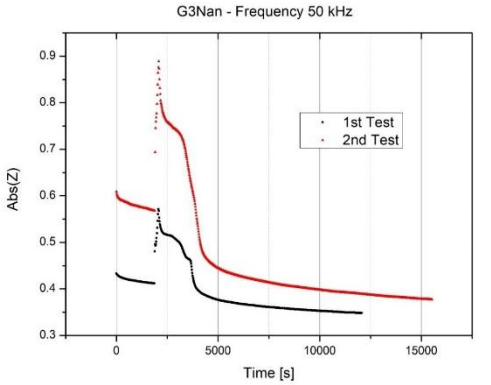

Figure 18. G3Nan, time dependence of Abs(Z) at 50 kHz.

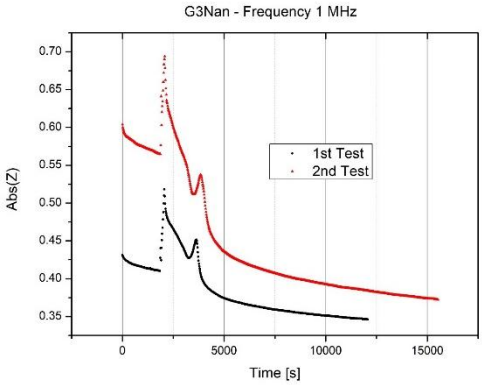

Figure 19. G3Nan, time dependence of Abs(Z) at 1 MHz.

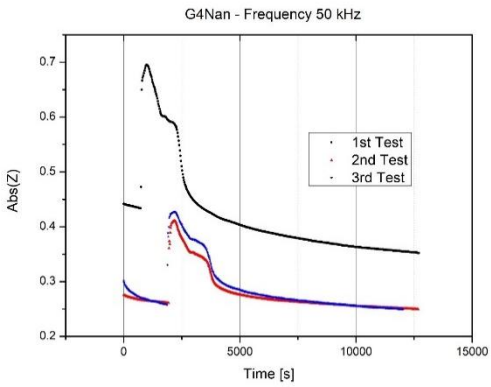

Figure 20. G4Nan, time dependence of Abs(Z) at 50 kHz.

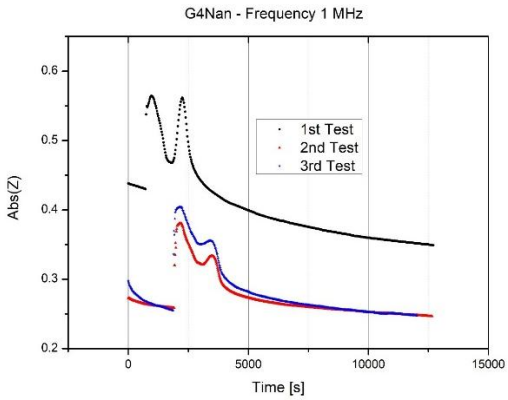

Figure 21. G4Nan, time dependence of Abs(Z) at 1 MHz.

From the above graphs, it can be seen that the Abs(Z) curve tends, after the initial surge due to the release of acetonitrile (which occurs around 1,800 s), to stabilize within 5,000 s, which corresponds to

about 50 min after release.

In the Abs(Z) curves, there are, however, several problems:

- Not all of them start from the same impedance value and no correlation is visible between the different values calculated in the different tests performed;
- The frequency dependence does not make the curves regular, especially for those at high frequencies (1 MHz);
- The final impedance values are usually different from the initial ones.

These problems are also found in **Table 2**. In the table, the following values of Abs(Z) have been selected:

- initial, equal to the average of the values calculated from the MFIA meter power-up to the time of release (thus 30 min);
- release;
- after 15 min, equal to 900 s from release;
- after 30 min, equal to 1,800 s from release;
- after 1 h, equal to 3,600 s from release;
- after 2 h, equal to 7,200 s from release.

The reference frequency is 50 kHz because, as mentioned earlier, at low frequencies, the curves tend to be more regular.

Next to the value of Abs(Z), there is its percentage value, established in the range that varies from the initial value and the maximum point obtained during the release phase of the organic substance.

Table 2. Values of Abs(Z) at the reference frequency of 50 kHz

(Frequency = 50 kHz)		**G2Nan**		**G3Nan**		**G4Nan**	
		Abs(Z)	**Percentage**	**Abs(Z)**	**Percentage**	**Abs(Z)**	**Percentage**
1st test	Initial	0.54774	0	0.41605	0	0.43705	0
	Release	0.82347	100	0.57156	100	0.69511	100
	After 15 min	0.74348	70.98974	0.50505	57.23105	0.59532	61.33070
	After 30 min	0.65852	40.17698	0.40843	−4.90001	0.46182	9.59854
	After 1 h	0.6129	23.63181	0.37106	−28.93062	0.40946	−10.69131
	After 2 h	0.59107	15.71465	0.355	−39.25793	0.3738	−24.50980
2nd test	Initial	0.57837	0	0.57666	0	0.26446	0
	Release	0.94365	100	0.88898	100	0.41087	100
	After 15 min	0.8012	61.00252	0.7406	52.49103	0.35029	58.62304
	After 30 min	0.67368	26.09231	0.57691	0.08005	0.29362	19.91667
	After 1 h	0.59391	4.254271	0.43246	−46.17059	0.27005	3.81805
	After 2 h	0.56059	−4.86750	0.40175	−56.00346	0.25738	−4.83574
3rd test	Initial	0.49303	0			0.26947	0
	Release	0.85536	100			0.42716	100
	After 15 min	0.74755	70.24536			0.37514	67.01122
	After 30 min	0.64928	43.12367			0.30658	23.53352
	After 1 h	0.58137	24.38109			0.27652	4.470797
	After 2 h	0.5599	18.45556			0.25804	−7.24840

The dependence of the Abs(Z) curve on frequency can only depend on the behavior of one of its two components, the real part Z' and the imaginary part Z''.

$$Z = Z' + jZ''$$

Figure 22 below allows us to understand that the frequency dependence comes mainly from the real part of the impedance Z', which follows almost at every point the trend of Abs(Z), thus forming in turn the depression caused by high frequencies (in this case 1 MHz).

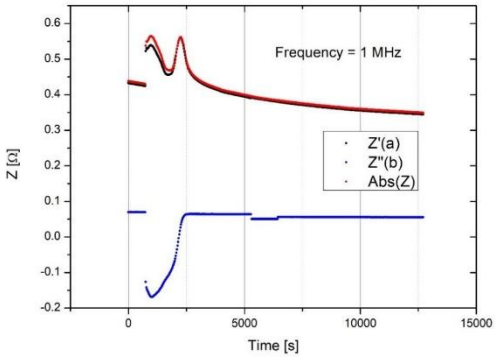

Figure 22. Time dependence of the real and the imaginary parts of the impedance *Z*, at the reference frequency of 1 MHz.

The imaginary part Z'', less affected by the frequency, shows a very regular curve, in which the final values are close to the initial ones. For this reason, it has been taken as a reference in **Figures 23**–**25**. For visual purposes, in the graphs, the value of the imaginary part shown will be $\left|\frac{1}{1+Z^{II}}\right|$.

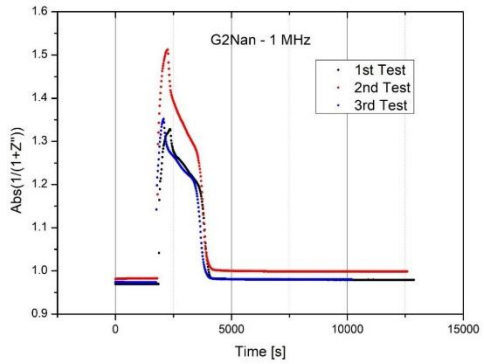

Figure 23. Time dependence for G2Nan, at the frequency of 1 MHz.

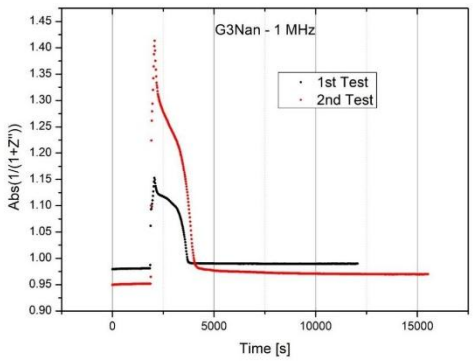

Figure 24. Time dependence for G3Nan, at the frequency of 1 MHz.

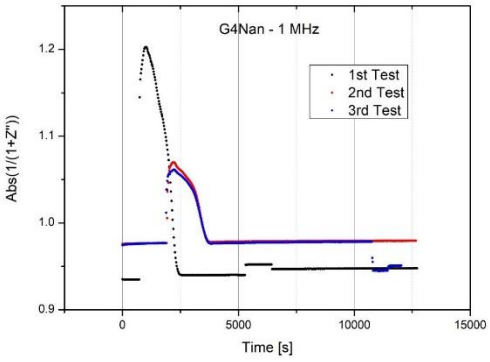

Figure 25. Time dependence of Abs(1/(1+Z'') for G4Nan, at the frequency of 1 MHz.

In **Table 3** (as it was done in **Table 2**), certain values of Abs(1/(1+Z'') and their reference percentages have been taken into account.

Table 3. Values of Abs(1/1+Z'') at the reference frequency of 1 MHz

(Frequency = 1 MHz)		**G2Nan**		**G3Nan**		**G4Nan**	
		Abs(1/1+Z'')	**Percentage**	**Abs(1/1+Z'')**	**Percentage**	**Abs(1/1+Z'')**	**Percentage**
1st test	Initial	0.96959	0	0.98036	0	0.93482	0
	Release	1.32846	100	1.15287	100	1.20272	100
	After 15 min	1.22302	70.61888	1.10348	71.36977	1.09462	59.64912
	After 30 min	0.98264	3.63641	0.99076	6.02863	0.9398	1.85890
	After 1 h	0.98012	2.93421	0.98984	5.49533	0.94005	1.95222
	After 2 h	0.97962	2.79488	0.98964	5.37939	0.94712	4.59126
2nd test	Initial	0.98224	0	0.95113	0	0.97639	0
	Release	1.51257	100	1.41321	100	1.06982	100
	After 15 min	1.31348	62.45922	1.2376	61.99575	1.03621	64.02654
	After 30 min	1.01198	5.60782	1.04427	20.15668	0.97805	1.77673
	After 1 h	0.9993	3.21686	0.9753	5.23069	0.97868	2.45103
	After 2 h	0.99866	3.09618	0.97126	4.35638	0.97936	3.17885
3rd test	Initial	0.97363	0			0.9761	0
	Release	1.35176	100			1.0615	100
	After 15 min	1.23131	68.14587			1.03219	65.67915
	After 30 min	0.99927	6.78073			0.97634	0.28103
	After 1 h	0.98095	1.93584			0.97729	1.39344
	After 2 h	0.98032	1.76923			0.97801	2.23653

From the percentages in **Table 3** it is evident that, for all types of graphene (G2Nan, G3Nan and G4Nan), 30 min after the release of acetonitrile, the values of Z'' have returned almost completely to their original values, which implies the total evaporation of our organic compound.

In the curves depicting the behavior of Z'', there are small "jumps", which can also be seen in **Figure 26** and **Figure 27**. These small deviations allow us to understand the sensitivity of the MFIA instrumentation, because they are most likely due to imperceptible movements or vibrations in the vicinity of the conductive plates that contain the membrane.

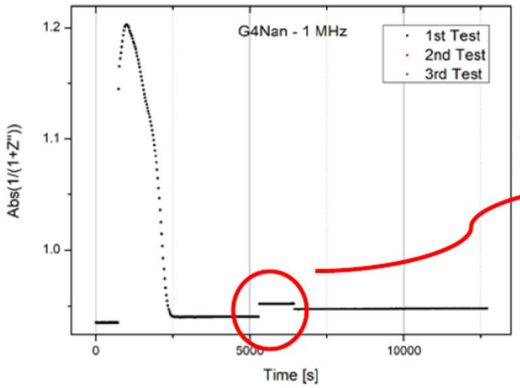

Figure 26. Evidence of small jumps in the time dependence of **Figure 25**.

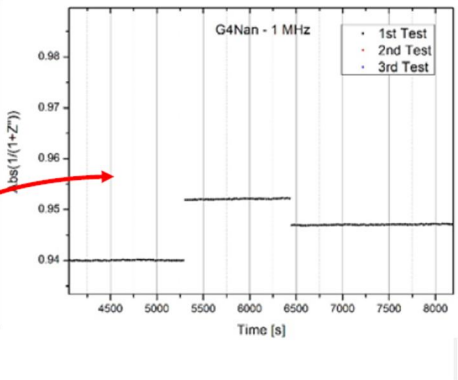

Figure 27. Magnified view of the inset in **Figure 26**.

Furthermore, we can conclude that all types of graphene show excellent adsorption properties, with virtually total evaporation of the absorbed acetonitrile after about 30–40 min after its release inside our filters (**Table 3** and **Figures 23**–**25**), also clear from the total absence of additional weight at the end of processing (**Table 1**).

Clearly, more work is needed to optimize, from the industrial viewpoint such devices, e.g., in testing the additional feature of being fully renewable and then regenerating them, in view of their possible use in relation to industrial processes, where industrial solvents and paints are involved. Nevertheless, the present device already represents a low-cost and ecologically friendly method to obtain the needed nanomaterial and the related membranes, to be employed as filters.

4. Conclusions

The study shows, first of all, that all types of graphene show excellent adsorption properties. Moreover, it leads to the following conclusions, i.e., that among the three types of graphene seen, G2Nan shows the greatest stability, evident from the virtually no decrease in weight during measurements (as seen in **Table 1**) and the lack of breakage of the membrane (unlike G3Nan and G4Nan). The results we obtained in the present investigation, corroborate the idea that graphene materials yield is a valid candidate for the absorption and removal of pollutants in water, owing to their high adsorbing capacities towards pollutants, which appear to be due to the effect of a large surface area available.

Acknowledgments

We acknowledge the participation of A. Lustrissimi and the support and encouragement by F. Bertocchi during the early stages of this work,

Data availability statement

Data are available by the author.

Conflicts of interest

The author declares no conflict of interest.

References

1. Chuanuwatanakul S, Dungchai W, Chailapakul O, Motomizu S. Determination of trace heavy metals by sequential injection-anodic stripping voltammetry using bismuth film screen-printed printed carbon electrode. Analytical Sciences 2008; 24(5): 589–594. doi: 10.2116/analsci.24.589.
2. Sui Zh, Meng Q, Zhang X, *et al.* Green synthesis of Carbon nanotube-graphene hybrid aerogels and their use as versatile agents for water purification. Journal of Materials Chemistry 2012; 22(18): 8767–8771. doi: 10.1039/C2JM00055E.
3. Wang H, Yuan X, Wu Y, *et al*. Adsorption characteristics and behaviors of graphene oxide for Zn(II) removal from aqueous solution. Applied Surface Science 2013; 279: 432–440. doi: 10.1016/j.apsusc.2013.04.133.
4. Ferrari AC, Meyer JC, Scardaci V, *et al*. Raman spectrum of graphene and graphene layers. Physical Review Letters 2006; 97(18): 87401. doi: 10.1103/PhysRevLett.97.187401.
5. Ferrigno L, Cataldo A, Sibilia S, *et al.* A monitorable and renewable pollution filter based on graphene nanoplatelets. Nanotechnology 2020; 31: 075701. doi: 10.1088/1361-6528/ab5072.
6. Miele G, Bellucci S, Cataldo A, *et al.* Electrical impedance spectroscopy for real-time monitoring of the life cycle of graphene nanoplatelets filters for some organic industrial pollutants. Transactions on Instrumentation and Measurement 2021; 70: 1503912. doi: 10.1109/TIM.2021.3089247.
7. Gomez CV, Guevara M, Tene T, *et al.* The liquid exfoliation of graphene in polar solvents. Applied Surface Science 2021; 546: 149046. doi: 10.1016/j.apsusc.2021.149046.
8. Sibilia S, Bertocchi F, Chiodini S, *et al.* Temperature-dependent electrical resistivity of macroscopic graphene nanoplatelet strips. Nanotechnology 2021; 32: 275701. doi: 10.1088/1361-6528/abef95.
9. Nanesa [Internet]. Available from: http://nanesa.com/en-US/Graphene.
10. Dabrowska A, Bellucci S, Cataldo A, *et al.* Nanocomposites of epoxy resin with graphene nanoplates and exfoliated graphite: Synthesis and electrical properties. Basic Solid State Physics 2014; 251(12): 2599–2602. doi: 10.1002/pssb.201451175.
11. Bellucci S. Study of graphene epoxy/nanoplatelets thin films subjected to aging in corrosive environments. Journal of Composites Science 2022; 6(2): 39. doi: 10.3390/jcs6020039.
12. Almasian A, Mahmoodi NM, Olya ME. Tectomer grafted nanofiber: Synthesis, characterization and dye removal ability from multicomponent system. Journal of Industrial and Engineering Chemistry 2015; 32: 85–98. doi: 10.1016/j.jiec.2015.08.002.
13. Mahmoodi NM, Ghezelbash M, Shabanian M, *et al.* Efficient removal of cationic dyes from colored wastewaters by dithiocarbamate-functionalized graphene oxide nanosheets: From synthesis to detailed kinetics studies. Journal of the Taiwan Institute of Chemical Engineers 2017; 81: 239–246. doi: 10.1016/j.jtice.2017.10.011.
14. Hosseini F, Sadighian S, Monfared HH, Mahmoodi NM. Dye removal and kinetics of adsorption by magnetic chitosan nanoparticles. Desalination and Water Treatment 2016; 57: 24378–24386. doi: 10.1080/19443994.2016.1143879.
15. Almasian A, Olya ME, Mahmoodi NM. Preparation and adsorption behavior of diethylenetriamine/polyacrylonitrile composite nanofibers for a direct dye removal. Fibers and Polymers 2015; 16(9): 1925–1934. doi: 10.1007/s12221-015-4624-3.
16. Hayati B, Mahmoodi NM, Arami M, Mazaher F. Dye removal from colored textile wastewater by poly(propylene imine) dendrimer: Operational parameters and isotherm studies. Clean Soil, Air, Water 2011; 39: 673–679. doi: 10.1002/clen.201000182.
17. Mahmoodi NM, Bashiri M, Moeen SJ. Synthesis of nickel–zinc ferrite magnetic nanoparticle and dye degradation using photocatalytic ozonation. Materials Research Bulletin 2012; 47: 4403–4408. doi: 10.1016/j.materresbull.2012.09.036.
18. Mahmood NM. Equilibrium, kinetics, and thermodynamics of dye removal using alginate in binary systems. Research on Chemical Intermediates 2015; 41: 3743–3757. doi: 10.1021/je101276x.
19. Mahmoodi NM. Synthesis of magnetic carbon nanotube and photocatalytic dye degradation ability. Environmental Monitoring and Assessment 2014; 186: 5595–5604. doi: 10.1007/s10661-014-3805-7.
20. Mahmoodi NM, Hayati B, Bahrami H, Arami M. Dye adsorption and desorption properties of Mentha pulegium in single and binary systems. Journal of Applied Polymer Science 2011; 122: 1489–1499. doi: 10.1002/app.34235.
21. Sharam R, Leila M, Mazaheri F, Mahmoodi NM. Degumming of Persian silk with mixed proteolytic enzymes. Journal of Applied Polymer Science 2007; 106: 267–275. doi: 10.1002/app.26492.
22. Mahmoodi NM, Moghimi F, Arami M, *et al.* Silk degumming using microwave irradiation as an environmentally friendly surface modification method. Fibers and Polymers 2010; 11: 234–240. doi: 10.1007/S12221-010-0234-2.
23. Mahmoodi NM, Saffar-Dastgerdi MH, Hayati B. Environmentally friendly novel covalently immobilized enzyme bionanocomposite: From synthesis to the destruction of pollutant. Composites Part B: Engineering 2020; 184: 107666. doi: 10.1016/j.compositesb.2019.107666.
24. Asefi D, Arami M, Sarabi AA, Mahmoodi NM. The chain length influence of cationic surfactant and role of nonionic co-surfactants on controlling the corrosion rate of steel in acidic media. Corrosion Science 2009; 51(8): 1817–1821. doi: 10.1016/j.corsci.2009.05.007.